RSC Advances

PAPER

View Article Online
View Journal | View Issue

Cite this: *RSC Adv.*, 2024, **14**, 38345

Effect of rare-earth ytterbium doping on the microwave absorption performance of nickel–cobalt ferrite

Guangming Wang,[a] Zhijun Ma, *[ab] Yunsheng Zheng,[a] Liang Cheng,[a] Huiling Xing[a] and Zhuomin Li[a]

Received 24th August 2024
Accepted 5th November 2024

DOI: 10.1039/d4ra06136e

rsc.li/rsc-advances

In order to investigate the effect of different doping proportions of Yb^{3+} on the structure and microwave absorption properties of ferrite, a sol–gel method was proposed to prepare spinel $Ni_{0.5}Co_{0.5}Yb_xFe_{2-x}O_4$. The crystal shape, particle size, elements, microstructure, electromagnetic loss and microwave absorption properties of $Ni_{0.5}Co_{0.5}Yb_xFe_{2-x}O_4$ were characterized by X-ray diffraction, inductively coupled plasma emission spectrometry, transmission electron microscopy, scanning electron microscopy and vector network analysis. Results show that nickel–cobalt–ytterbium ferrite microwave absorbing materials can be prepared under optimal conditions, with an average particle size of 38.00–45.00 nm. With the increase in the doping amount, the microwave absorption performance first increases and then decreases. When Yb^{3+} = 0.02, $Ni_{0.5}Co_{0.5}Yb_{0.02}Fe_{1.98}O_4$ has the best microwave absorption performance, the best reflection loss is −21.04 dB, and the effective microwave absorption bandwidth in the Ku band is 2.55 GHz (15.45–18.00 GHz). The prepared nickel–cobalt–ytterbium ferrite microwave absorbing material has the advantages of less thickness, light weight, strong reflection loss and simple synthesis method. The excellent absorbing properties of $Ni_{0.5}Co_{0.5}Yb_{0.02}Fe_{1.98}O_4$ are attributed to the interaction between natural resonance and exchange resonance.

Introduction

With the development and progress of the information age, the problems of human health and ecological environment caused by electromagnetic pollution have attracted much attention.[1,2] Therefore, it is of great significance to research, design and develop microwave absorbing materials for preventing and treating electromagnetic pollution.[3–5] For national defense science and technology, the study of microwave absorbing materials is conducive to the development of China's cutting-edge stealth technology and can identify the "soft rib" of stealth technology to strengthen the national defense force.[6–8] After years of development, many excellent microwave absorbing materials have been discovered, such as ferrite,[9] barium titanate,[10] polycrystalline iron fibers,[11] and graphite materials.[12] Among them, ferrite can absorb electromagnetic waves in high frequency, ultra-high frequency and microwave frequency bands.[13] It can also be reused without affecting its microwave absorption performance, good corrosion resistance[14] and high temperature resistance.[15] Ferrite is suitable for use in various environments and has several other advantages. Therefore, it has very high research value for civil and military purposes.

At present, ferrite preparation methods include liquid phase method, gas phase method and solid phase method. The liquid phase method has the advantages of high purity, good uniformity and accurate chemical composition control. The liquid phase method includes sol–gel method, hydrothermal method and chemical coprecipitation method.[16,17] Ferrite materials prepared by hydrothermal method and chemical coprecipitation methods have the disadvantages of serious grain agglomeration and high density, and it is difficult to meet the requirements of "light, thin, wide and strong" microwave absorbing materials.[18] The sol–gel method has the characteristics of easy control of material composition, good rheological properties, molecular level uniformity in a short time, and light product. Xiaogang Su *et al.*[19] prepared rare earth Gd^{3+}-doped ferrite ($Gd_xFe_{3-x}O_4$) microwave absorbing material by a solvothermal method. When the doping amount was x = 0.02, thickness = 5.1 mm, and frequency = 6.1 GHz, the minimum reflection loss was −48.90 dB. The effective absorption bandwidth was 5.53 GHz (2.79–6.77 GHz, 15.52–17.07 GHz). Hongwei Chen *et al.*[20] prepared nano-$M_{0.4}Zn_{0.6}Pr_xFe_{2-x}O_4$ microwave absorbing materials doped with rare earth Pr^{3+} by hydrothermal synthesis method. For a doping amount of x = 0.03 and frequency = 16–18 GHz, the minimum reflection loss was −19.216 dB. Lei Guo *et al.*[21] prepared Nd^{3+}-doped spinel type

[a]College of Mining, Liaoning Technical University, Fuxin 123000, China. E-mail: zhijunma0930@126.com
[b]College of Materials Science & Engineering, Liaoning Technical University, Fuxin 12300, China

$NiNd_xFe_{2-x}O_4$ microwave absorbing material by the sol–gel method. When the doping amount was $x = 0.02$, thickness = 6.02 mm, and frequency = 7.92 GHz, the minimum reflection loss was −47 dB and the effective absorption bandwidth was 4.5 GHz.

In summary, spinel ferrites doped with rare earths have good wave-absorbing properties, and there are few research articles on rare earth ytterbium. Hence this study chooses rare earth ytterbium doped nickel–cobalt ferrite to study its wave absorbing properties.

Experimental

Materials

(1) Reagents: $C_6H_8O_7 \cdot H_2O$, $Ni(NO_3)_2 \cdot 6H_2O$, $Co(NO_3)_2 \cdot 6H_2O$, $Fe(NO_3)_3 \cdot 9H_2O$, $Yb(NO_3)_3 \cdot 5H_2O$, $NH_3 \cdot H_2O$, all analytical grade (AR), distilled water.

(2) Instrument: X-ray diffractometer (XRD), a D8 ADVANCE model. Inductively coupled plasma emission spectrometer (ICP-OES), Agilent 5110 model. Transmission electron microscope (TEM), JEM-2010 model. Scanning electron microscope (SEM), GeminiSEM 300 model. Vector Network Analysis (VNA), HP8722ES type.

Experimental: synthesis steps

(1) The metal ions of nitrate and citric acid were weighed in a 1 : 1 ratio (the doping ratio of Yb^{3+} in ferrite is $Ni_{0.5}Co_{0.5}Yb_xFe_{2-x}O_4$ (x = 0.00, 0.02, 0.04, 0.06, 0.08)) and mixed in 50 mL distilled water.

(2) Ultrasonic dispersion was carried out with an ultrasonic cleaner, ultrasonic treatment was performed for 10 min, stirring by glass rod was done, and then ultrasonic treatment was continued for 10 min.

(3) The obtained mixed solution was poured into a four-mouth flask and stirred in a constant temperature water bath at 80 °C for 10 min. Ammonia water was added at the rate of 3 s per drop, the pH was adjusted to 7 and then stirred in a constant temperature water bath for 4 h; the speed was 120 rpm.

(4) The sol was put into a vacuum drying oven and dried at 120 °C for 4 h to obtain the gel, then cooled at room temperature for 15 min.

(5) The gel was placed in a muffle oven, heated to 200 °C at 15 °C min^{-1} and kept warm for 5 min.

(6) The obtained product was ground and placed in a muffle furnace. It was heated to 950 °C at a rate of 5 °C min^{-1} and kept at that temperature for 180 minutes to obtain nano nickel–cobalt–ytterbium ferrite.

Characterization

(1) The phase composition of the sample was tested using a D8 ADVANCE X-ray diffractometer (XRD). The conditions were: Cu target Kα radiation, wavelength 0.15406 nm, working voltage 40 kV, tube current 30 mA, scanning speed 10° min^{-1}, scanning range 5–80°.

(2) An Agilent 5110 inductively coupled plasma emission spectrometer (ICP-OES) was used to analyze the elemental content of the samples. The power was 1250 W, the plasma gas flow was 12.0 L min^{-1}, the auxiliary gas flow was 1.0 L min^{-1}, the atomizer gas flow was 0.70 L min^{-1}, and three replicates were recorded.

(3) The morphology and particle size of the crystals were analyzed by a JEM-2010 transmission electron microscope (TEM). The resolution was 0.1–0.2 nm, the acceleration voltage was 200 kV, and the magnification was 20×–1 000 000×.

(4) The morphology of the samples was analyzed by a GeminiSEM 300 scanning electron microscope (SEM). The resolution was 0.8–1.4 nm and the magnification was 12–2 000 000×.

(5) The complex permittivity and complex permeability of the samples in the frequency range of 0–18 GHz were measured by the coaxial line method using an HP8722ES vector network analyzer (VNA). The sample powder was mixed with paraffin wax in a ratio of 7 : 3. After mixing evenly, it was pressed into a ring with a mold to make a circular composite material with a thickness of 2 mm. The electromagnetic parameters of the samples were determined by a vector network analyzer.

Results and discussion

Crystal structure analysis

Fig. 1 shows the XRD characterization results of Yb^{3+} with different doping ratios. The diffraction peak intensity of each doping ratio is roughly the same, indicating that the crystallization effect of ferrite prepared by the sol–gel method is better. The 2θ diffraction angles are 18.4°, 30.3°, 35.7°, 37.3°, 43.4°, 53.8°, 57.4°, 63.0°, 71.5°, 74.6°, and 75.6° corresponding to the (111), (220), (311), (222), (400), (422), (511), (440), (620), (533), and (622) crystal planes. The diffraction peak of the sample was compared with PDF#86-2267 standard card, and no miscellaneous peak appeared.[22] The results show that pure spinel-type nickel–cobalt–ytterbium ferrite has been prepared. From the XRD patterns in Fig. 1, it can be seen that the strongest diffraction peak intensity is the (311) crystal plane, indicating that the preferred crystallization orientation of the crystal is (311). The distance between the crystal faces of the sample (d) was calculated according to Bragg's formula. The mean particle

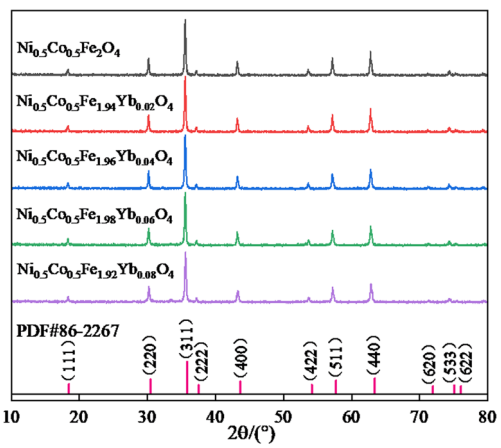

Fig. 1 XRD curves for doping with different Yb^{3+} ratios.

size (D) and lattice constant (α) of the sample were calculated according to Scherrer's formula.

$$n\lambda = 2d\sin\theta \quad (1)$$

$$D = k_1\lambda/\beta\cos\theta \quad (2)$$

$$\alpha = \lambda\sqrt{h^2 + k^2 + l^2}\Big/2\sin\theta \quad (3)$$

In the formula, λ is the wavelength, which is 0.154056; n is the reflection series, which is 1; k_1 is the correction coefficient, which is 0.89; β is the half-peak width of the main diffraction peak; θ is the diffraction angle; and h, k, and l are the crystal face indices. The calculated structural parameters are shown in Table 1. It can be seen from Table 1 that after Yb^{3+} doping, the 2θ diffraction angle of (311) crystal surface shifts to the left as a whole. However, with the increase in the Yb^{3+} doping ratio, the 2θ diffraction angle moves to the right. The lattice constant gradually decreases from 0.8374 to 0.8361. The grain size decreased significantly, decreasing by 23.3–29.2 nm. The reason is that the growth of nickel–cobalt ferrite is limited by the substitution of Yb^{3+}; because Yb^{3+} has a large radius, it will preferentially enter the octahedral position with a large nickel–cobalt ferrite gap, causing lattice distortion, and the internal stress generated by it will limit the growth of crystals. Therefore, it was observed that the grain size of doped Yb^{3+} nickel–cobalt ferrite is smaller. However, with the increase in the Yb^{3+} doping ratio, the grain size gradually increases, indicating that Yb^{3+} gradually replaces Fe^{3+} in the spinel structure, which is consistent with the increase in the Yb^{3+} doping ratio. Therefore, doping with different Yb^{3+} will affect the structural parameters of ferrite.

According to the comprehensive analysis in Fig. 1 and Table 1, sample $Ni_{0.5}Co_{0.5}Yb_{0.02}Fe_{1.98}O_4$ has the best crystallinity, the strongest diffraction peak and the smallest grain size. Therefore, the content of the main elements in $Ni_{0.5}Co_{0.5}Yb_{0.02}Fe_{1.98}O_4$ was detected, as shown in Fig. 2.

According to the analysis in Fig. 2, the contents of Fe, Ni, Co and Yb are 46.32%, 12.45%, 12.61% and 0.48%, respectively. The ratio between the elements is approximately 99 : 25 : 25 : 1, which meets the stoichiometric ratio of $Ni_{0.5}Co_{0.5}Yb_{0.02}Fe_{1.98}O_4$, thus proving that the types and contents of elements in the sample conform to the characteristics of $Ni_{0.5}Co_{0.5}Yb_{0.02}Fe_{1.98}O_4$.

Table 1 Structure parameters of nickel–cobalt–ytterbium ferrite

				(311) priority crystallization diffraction peak	
Structural formula	2θ/(°)	d/nm	α/nm	FWHM/(°)	D/nm
$Ni_{0.5}Co_{0.5}Fe_2O_4$	35.67	0.2515	0.8341	0.00213	67.6
$Ni_{0.5}Co_{0.5}Yb_{0.02}Fe_{1.98}O_4$	35.52	0.2525	0.8374	0.00375	38.4
$Ni_{0.5}Co_{0.5}Yb_{0.04}Fe_{1.96}O_4$	35.53	0.2524	0.8371	0.00363	39.7
$Ni_{0.5}Co_{0.5}Yb_{0.06}Fe_{1.94}O_4$	35.54	0.2523	0.8367	0.00346	41.6
$Ni_{0.5}Co_{0.5}Yb_{0.08}Fe_{1.92}O_4$	35.57	0.2521	0.8361	0.00325	44.3

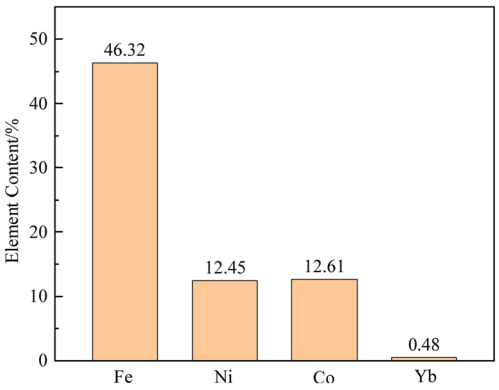

Fig. 2 Histogram of the elemental content of $Ni_{0.5}Co_{0.5}Yb_{0.02}Fe_{1.98}O_4$.

Morphological analysis

Fig. 3 shows the TEM characterization results of $Ni_{0.5}Co_{0.5}Yb_xFe_{2-x}O_4$ sample. As can be seen from the figure, the ferrite doped with Yb^{3+} has an irregular structure, and the average grain size can reach 38–45 nm, which is basically consistent with the results calculated by Scherrer's formula in XRD. However, the crystal surface could not be observed from the TEM results; thus, the sample of $Ni_{0.5}Co_{0.5}Yb_xFe_{2-x}O_4$ was tested by SEM, and the results are shown in Fig. 4. It can be clearly seen from Fig. 4 that the grain size of the ferrite doped with Yb^{3+} is significantly smaller than that without doping, which corresponds to the results in Table 1. The overall appearance of an irregular shape and flat surface is consistent with the TEM results. However, its dispersion is poor and its distribution is uneven. The reason is that the nickel–cobalt–ytterbium ferrite particles have magnetic attraction and intermolecular force, and the particles attract each other and connect into larger aggregates. At the same time, the magnetostatic energy is reduced, and the growth rate is difficult to control, resulting in uneven distribution.

Microwave-absorbing performance analysis

Fig. 5 shows the relationship between reflection loss, frequency and thickness of the $Ni_{0.5}Co_{0.5}Yb_xFe_{2-x}O_4$ sample. According to formula (4), (5), (6), (7),[23,24] the relation curve between microwave absorption reflectivity and frequency is calculated as follows.

$$R_L(\mathrm{dB}) = 20\lg|Z_{in} - Z_0)/(Z_{in} + Z_0)| \quad (4)$$

$$Z_{in} = Z_0\sqrt{\mu_r/\varepsilon_r}\tanh\left[j(2\pi fd/c)\sqrt{\mu_r\varepsilon_r}\right] \quad (5)$$

$$\varepsilon_r = \varepsilon' - j\varepsilon'' \quad (6)$$

$$\mu_r = \mu' - j\mu'' \quad (7)$$

In the formula, R_L—reflection loss; Z_{in}—microwave absorbing material transmission impedance; Z_0—free space transmission impedance; d—material thickness at test, m; f—frequency of incident electromagnetic waves, GHz; c—speed of light, roughly

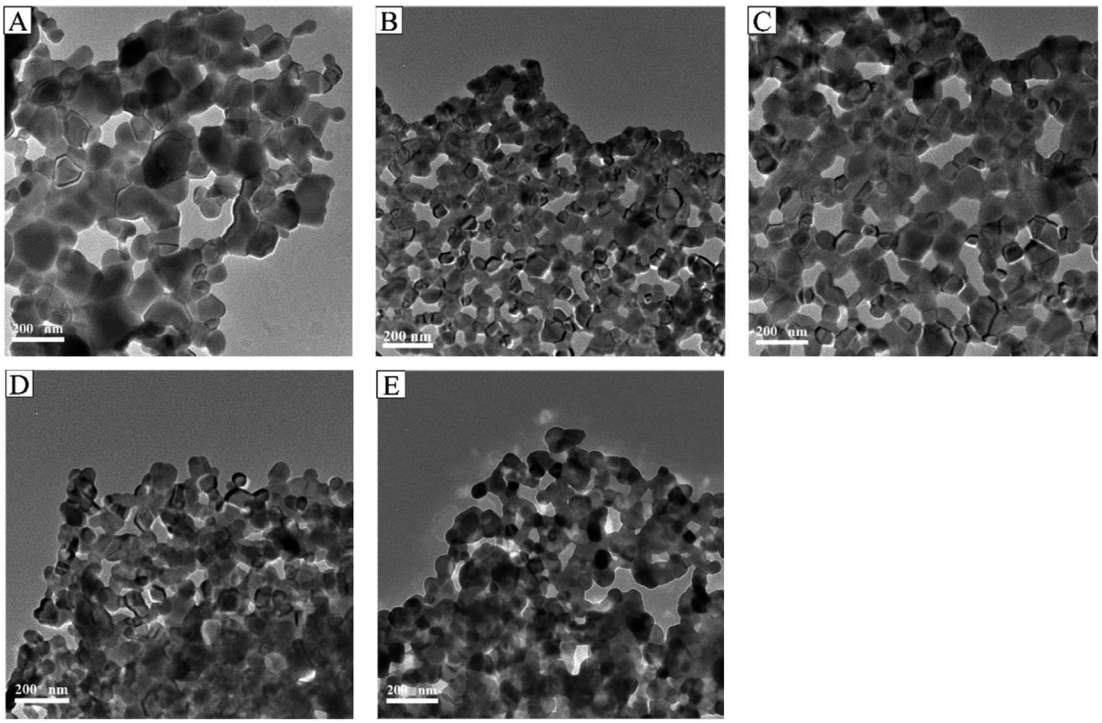

Fig. 3 TEM images of doping with different Yb^{3+} ratios ((A) $Ni_{0.5}Co_{0.5}Fe_2O_4$, (B) $Ni_{0.5}Co_{0.5}Yb_{0.02}Fe_{1.98}O_4$, (C) $Ni_{0.5}Co_{0.5}Yb_{0.04}Fe_{1.96}O_4$, (D) $Ni_{0.5}Co_{0.5}Yb_{0.06}Fe_{1.94}O_4$, (E) $Ni_{0.5}Co_{0.5}Yb_{0.08}Fe_{1.92}O_4$).

equal to 3×10^8 m s^{-1}; ε_r—complex permittivity; μ_r —complex permeability; ε''—real part of complex dielectric constant; ε'—imaginary part of complex dielectric constant; μ''—real part of complex magnetic permeability; μ'—imaginary part of complex magnetic permeability.

As can be seen from Fig. 5, with the increase in the Yb^{3+} doping ratio, the microwave absorption performance presents a trend of first increase and then decrease. When $Yb^{3+} = 0.00$, the minimum reflection loss is −16.15 dB at the absorption layer thickness of 3.0 mm and frequency of 17.32 GHz. When $Yb^{3+} = 0.02$, the minimum reflection loss is −21.04 dB at the absorption layer thickness of 2.5 mm and frequency of 17.15 GHz. When $Yb^{3+} = 0.04$, the minimum reflection loss is −7.17 dB at an absorption layer thickness of 3.5 mm and frequency of

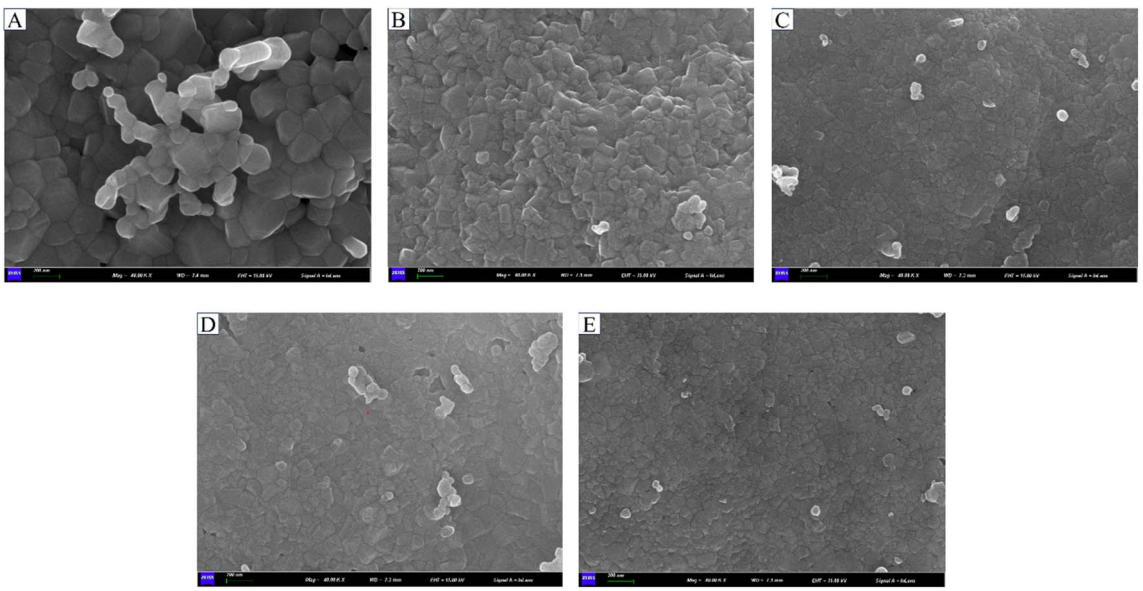

Fig. 4 SEM images of samples doped with different Yb^{3+} ratios ((A) $Ni_{0.5}Co_{0.5}Fe_2O_4$, (B) $Ni_{0.5}Co_{0.5}Yb_{0.02}Fe_{1.98}O_4$, (C) $Ni_{0.5}Co_{0.5}Yb_{0.04}Fe_{1.96}O_4$, (D) $Ni_{0.5}Co_{0.5}Yb_{0.06}Fe_{1.94}O_4$, (E) $Ni_{0.5}Co_{0.5}Yb_{0.08}Fe_{1.92}O_4$).

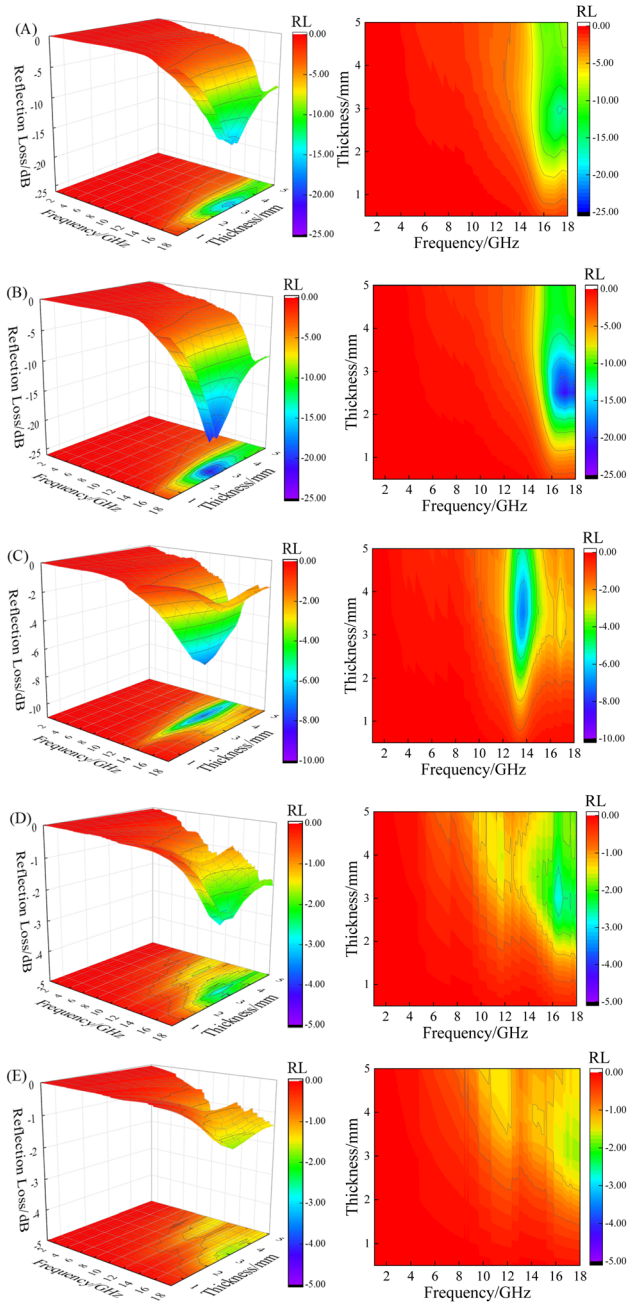

Fig. 5 Reflection loss, frequency, and thickness relationship curves with different Yb^{3+} doping ratios ((A) $Ni_{0.5}Co_{0.5}Fe_2O_4$, (B) $Ni_{0.5}Co_{0.5}Yb_{0.02}Fe_{1.98}O_4$, (C) $Ni_{0.5}Co_{0.5}Yb_{0.04}Fe_{1.96}O_4$, (D) $Ni_{0.5}Co_{0.5}Yb_{0.06}Fe_{1.94}O_4$, (E) $Ni_{0.5}Co_{0.5}Yb_{0.08}Fe_{1.92}O_4$).

13.75 GHz. When $Yb^{3+} = 0.06$, the minimum reflection loss is −2.87 dB at an absorption layer thickness of 3.0 mm and frequency of 16.47 GHz. When $Yb^{3+} = 0.08$, the minimum reflection loss is −1.72 dB at the absorption layer thickness of 3.0 mm and frequency of 17.41 GHz. When doped with $Yb^{3+} = 0.02$, the microwave absorption effect is the best, and the effective band width of <−10.00 dB is 2.55 GHz (15.45–18.00 GHz). The reason why $Ni_{0.5}Co_{0.5}Yb_{0.02}Fe_{1.98}O_4$ has better microwave absorption performance is that in nano $Ni_{0.5}Co_{0.5}Yb_xFe_{2-x}O_4$, Yb^{3+} preferentially occupies the octahedral position (*i.e.*, B site) in each unit cell. As the proportion of Yb^{3+} doping increases, the lattice constant gradually decreases and the crystal orientation boundary decreases, resulting in a decrease in the demagnetization energy, an increase in magnetic moment, and an increase in hysteresis loss. When the doping ratio is too high, Yb^{2+} appears in the octahedron (B-site), and Yb^{3+} and Yb^{2+} electron exchange exists, while electron exchange between Fe^{3+} and Fe^{2+} disappears, resulting in the reduction of exchanged electrons, the weakening of electrical conductivity and the reduction of dielectric loss.[25] Therefore, the microwave absorption performance of $Ni_{0.5}Co_{0.5}Yb_xFe_{2-x}O_4$ can be effectively enhanced by doping the appropriate proportion.

Electromagnetic performance analysis. The tangent value of ferrite loss angle (tan δ) can be used to represent the value of electromagnetic wave loss. It contains the tangent value of the electrical loss angle (tan δ_e) and the tangent value of the magnetic loss angle (tan δ_m). Formula (8) (ref. 26) is as follows:

$$\tan\delta = \tan\delta_e + \tan\delta_m = (\varepsilon''/\varepsilon') + (\mu''/\mu') \quad (8)$$

In the formula, the ratio of the imaginary part ε'' to the real part ε' of the complex dielectric constant is tan δ_e, and the ratio of the imaginary part μ'' to the real part μ' of the complex magnetic permeability is tan δ_m. Also, the larger the tan δ value, the better the microwave absorbing performance of the material.

Fig. 6(A) and (B) respectively show the relationship curves of dielectric loss tangent value and magnetic loss tangent value of $Ni_{0.5}Co_{0.5}Yb_xFe_{2-x}O_4$ with frequency changes, both of which show nonlinear changes. It can be seen from Fig. 6(A) that when doped $Yb^{3+} = 0$, 0.02, 0.04, 0.06, ferrite has an obvious formant. In the frequency range of 1.00–17.00 GHz, the dielectric loss value of $Yb^{3+} = 0.02$ ferrite is higher than that of other doping

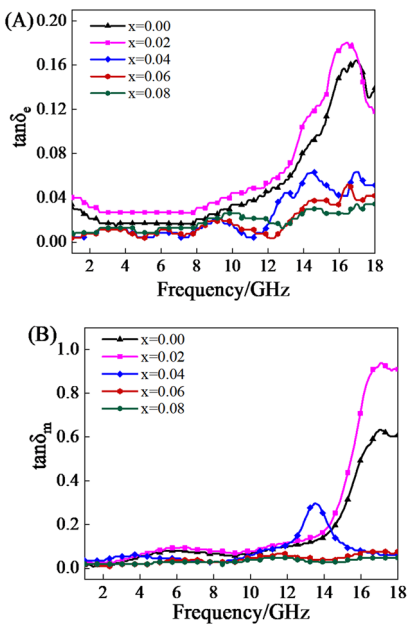

Fig. 6 Tan δ_e, tan δ_m and frequency relationship curves of doping with different Yb^{3+} proportions.

ratios. The maximum dielectric loss tangent value is 0.18 at a frequency of 16.73 GHz. It can be seen from Fig. 6(B) that when doped $Yb^{3+} = 0$ and 0.02, ferrite has an obvious formant. In the frequency range of 14.50–18.00 GHz, the magnetic loss value of $Yb^{3+} = 0.02$ ferrite is higher than that at other doping ratios. The maximum magnetic loss tangent value is 0.94 at a frequency of 17.15 GHz. In the whole frequency band, the tangent value curve of dielectric loss first increases and then decreases, but the overall trend is increasing, while the tangent value curve of magnetic loss shows a gradual increasing trend.

Fig. 7(A) shows the relationship between the loss angle tangent value and the frequency change of $Ni_{0.5}Co_{0.5}Yb_xFe_{2-x}O_4$, which presents a nonlinear change. $Ni_{0.5}Co_{0.5}Yb_{0.02}Fe_{1.98}O_4$ has the largest loss angle tangent value, which is $\tan\delta = 1.10$. It also verified that $Ni_{0.5}Co_{0.5}Yb_{0.02}Fe_{1.98}O_4$ has a higher loss factor, which is one of the reasons for its better microwave absorption performance compared with other doping ratios. The tangent value of the magnetic loss of $Ni_{0.5}Co_{0.5}Yb_{0.02}Fe_{1.98}O_4$ is greater than the tangent value of the electrical loss in the whole absorbing frequency band, which indicates that the dielectric loss is very small and the absorption of microwave mainly comes from the magnetic loss. Therefore, Fig. 7(B) analyzes the forms of magnetic loss at different frequency bands. Fig. 7(B) shows the relationship between magnetic loss C_0 and frequency variation of $Ni_{0.5}Co_{0.5}Yb_{0.02}Fe_{1.98}O_4$. According to formula (9),[27]

$$C_0 = \mu''/((\mu')^2 f) \quad (9)$$

It can be seen from the figure that the curve of the $Ni_{0.5}Co_{0.5}Yb_xFe_{2-x}O_4$ sample ($x = 0$, 0.02, 0.04, 0.06, 0.08) fluctuates in a wide range at low frequency in the range of 1.00–10.00 GHz, indicating the magnetic loss caused by natural resonance at this frequency. Natural resonance generally occurs at low frequency bands and is usually caused by shape anisotropy and magnetocrystalline anisotropy.[28,29] At frequencies ranging from 6.00 GHz to 18.00 GHz, the curves of samples $Ni_{0.5}Co_{0.5}Yb_{0.06}Fe_{1.94}O_4$ and $Ni_{0.5}Co_{0.5}Yb_{0.08}Fe_{1.92}O_4$ show a small fluctuation range, indicating the magnetic loss caused by eddy current loss at this frequency.[30] The samples $Ni_{0.5}Co_{0.5}Fe_2O_4$, $Ni_{0.5}Co_{0.5}Yb_{0.02}Fe_{1.98}O_4$ and $Ni_{0.5}Co_{0.5}Yb_{0.04}Fe_{1.96}O_4$ have obvious resonance peaks in the frequency range of 10.00–18.00 GHz, indicating the magnetic loss caused by exchange resonance. Exchange resonances generally occur at high frequency bands and are usually caused by surface anisotropy and energy exchange between grains.[31] Therefore, the magnetic loss form of $Ni_{0.5}Co_{0.5}Yb_{0.02}Fe_{1.98}O_4$ in this frequency band is the joint action of natural resonance and exchange resonance. The results show that different doping ratios can affect the magnetic loss form of nickel–cobalt–ytterbium ferrite.

High-quality microwave absorbing materials have two characteristics: attenuation properties and impedance matching. Attenuation characteristics mean that electromagnetic waves will be converted into other forms of energy after entering the material, and the higher the attenuation constant, the better the microwave absorption effect.[32] Impedance matching means that before electromagnetic waves enter the interior of the material, some electromagnetic waves will be reflected because the impedance matching between the air and the surface of the material is inconsistent. At the frequency with the best microwave absorption effect, the closer the impedance matching is to 1, the stronger the performance.[33]

Fig. 8 shows the relationship between the attenuation constant and frequency of the $Ni_{0.5}Co_{0.5}Yb_xFe_{2-x}O_4$ sample. Here, the attenuation constant is α, which is plotted according to formula (10).[34]

$$\alpha = \frac{\sqrt{2}\pi f}{c} \times \sqrt{(\mu''\varepsilon'' - \mu'\varepsilon') + \sqrt{(\mu''\varepsilon'' - \mu'\varepsilon')^2 + (\mu'\varepsilon'' - \mu''\varepsilon')^2}} \quad (10)$$

It can be seen from the figure that the peaks of $Ni_{0.5}Co_{0.5}Yb_{0.06}Fe_{1.94}O_4$ and $Ni_{0.5}Co_{0.5}Yb_{0.08}Fe_{1.92}O_4$ samples fluctuate

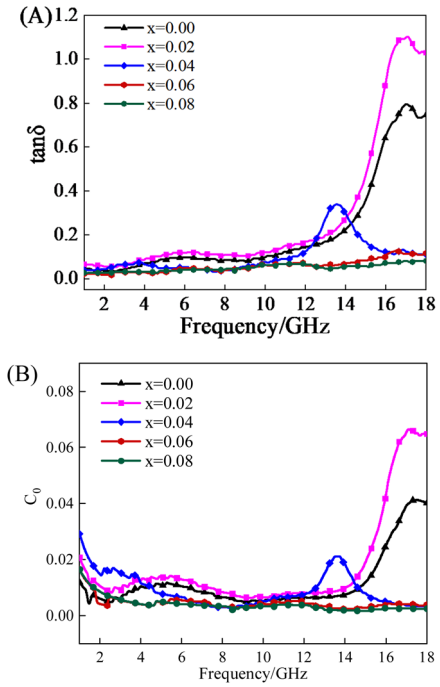

Fig. 7 Tan δ, C_0 and frequency relationship curve of $Ni_{0.5}Co_{0.5}Yb_xFe_{2-x}O_4$ sample.

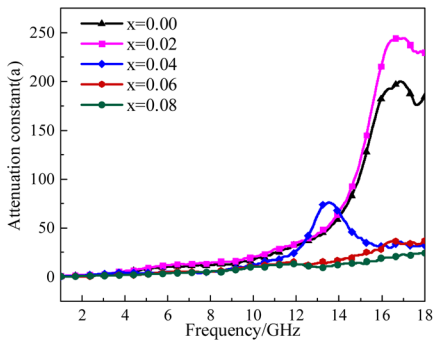

Fig. 8 Attenuation constant and frequency relationship curve of $Ni_{0.5}Co_{0.5}Yb_xFe_{2-x}O_4$ sample.

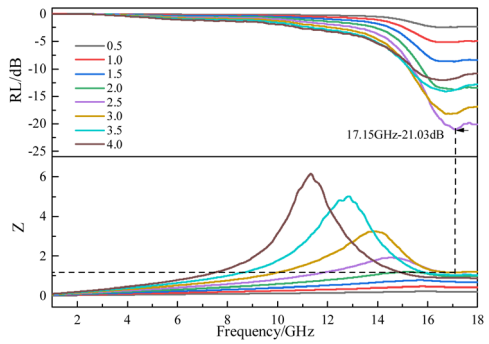

Fig. 9 Impedance matching, reflection loss and frequency relationship curve of the $Ni_{0.5}Co_{0.5}Yb_xFe_{2-x}O_4$ sample.

between 1.00 GHz and 18.00 GHz, but the fluctuations are not obvious. The attenuation constant of sample $Ni_{0.5}Co_{0.5}Yb_{0.02}Fe_{1.98}O_4$ is the highest, reaching 242.89 at a frequency of 17.15 GHz. This also confirms that the good absorption effect of sample $Ni_{0.5}Co_{0.5}Yb_{0.02}Fe_{1.98}O_4$ is due to its high attenuation constant.

Fig. 9 is the impedance matching diagram of the $Ni_{0.5}Co_{0.5}Yb_{0.02}Fe_{1.98}O_4$ sample. According to formula (11),[35]

$$Z = Z_{in}/Z_0 = \sqrt{\mu_r/\varepsilon_r}\tanh\left[j(2\pi fd/c)\sqrt{\mu_r\varepsilon_r}\right] \quad (11)$$

According to the above results, the $Ni_{0.5}Co_{0.5}Yb_{0.02}Fe_{1.98}O_4$ sample has the best microwave absorption effect and the largest attenuation constant. Therefore, only the impedance matching diagram of the $Ni_{0.5}Co_{0.5}Yb_{0.02}Fe_{1.98}O_4$ sample with different thicknesses is discussed here. It can be seen from the figure that when the absorption layer thickness of $Ni_{0.5}Co_{0.5}Yb_{0.02}Fe_{1.98}O_4$ is 2.5 mm and the frequency is 17.15 GHz, the minimum reflection loss value is −21.03 dB, and the impedance matching value Z is 1.16. Compared with the minimum reflection loss of other thicknesses, the impedance matching value at the corresponding frequency is closer to 1. It is also verified that $Ni_{0.5}Co_{0.5}Yb_{0.02}Fe_{1.98}O_4$ not only has a larger attenuation constant at the frequency with the best microwave absorption effect but the impedance matching is also closer to 1.

Conclusions

In summary, in this paper, the sol–gel method has been used to prepare pure spinel-type nickel–cobalt–ytterbium ferrite without impurity peaks under the conditions of solution pH 7, molar ratio of citric acid to metal ion = 1 : 1, crystallization temperature 950 °C and crystallization time 3 h. With the increase in the doping amount, the microwave absorption performance first increases and then decreases. Through the correlation calculation after XRD and the observation by transmission electron microscopy, it is mutually confirmed that the grain size is in the range of 38–45 nm. The microwave absorption performance is the best when doped with Yb^{3+} = 0.02. At an absorption layer thickness of 2.5 mm and frequency of 17.15 GHz, the reflection loss is the smallest, which is −21.03 dB. The effective microwave absorption frequency band is 2.55 GHz (15.45–18.00 GHz). Compared with undoped nickel–cobalt ferrite, the reflection loss is increased by 30.28%, and the microwave absorption performance is significantly improved. $Ni_{0.5}Co_{0.5}Yb_{0.02}Fe_{1.98}O_4$ is dominated by magnetic loss in the whole frequency band, and its magnetic loss mechanism is mainly the interaction of natural resonance and exchange resonance. At a frequency of 17.15 GHz, the attenuation constant α = 242.89 and the impedance matching Z = 1.16. These results show that Ni–Co ferrite doped with rare earth ytterbium has the advantages of thin thickness, low cost, strong reflection loss and simple synthesis method. It is a kind of microwave absorbing material with high application prospect.

Data availability

All the data from this study are available, and raw data can be provided for editors and reviewers.

Conflicts of interest

There are no conflicts to declare.

Acknowledgements

The authors would like to acknowledge the financial support received through the National Natural Science Foundation (52274265).

Notes and references

1 J. W. Zhang, X. Meng, X. F. Wei, G. Fu, C. Putson, B. Rabah, H. Abdelowahed and F. Belhora, *Sens. Actuators, A*, 2023, **363**, 114757.
2 B. S. Zhu, W. P. Mu, Y. F. Gao, G. M. Li and Y. M. Tian, *Surf. Interfaces*, 2023, **42**, 103354.
3 K. Mandeep, K. G. Sachin and B. Shalini, *J. Magn. Magn. Mater.*, 2024, **600**, 172158.
4 K. Parveen, N. Praveen, K. D. Alok, B. B. Himangshu, K. Sumit, K. M. Ashish and K. Ashavani, *Mater. Chem. Phys.*, 2024, **319**, 129360.
5 G. V. Kostishin, M. I. Isaev and V. D. Salogub, *Polym.*, 2024, **16**, 1003.
6 H. Ahmad, A. Tariq, A. Shehzad, M. S. Faheem, M. Shafiq, I. A. Rashid, A. Afzal, A. Munir, M. T. Riaz, H. T. Haider, A. Afzal, M. B. Qadir and Z. Khaliq, *Polym. Compos.*, 2019, **40**, 4457–4472.
7 V. G. Kostishyn, I. M. Isaev, R. I. Shakirzyanov, D. V. Salogub, A. R. Kayumova and V. K. Olitsky, *Tech. Phys.*, 2024, **68**, S178–S184.
8 I. M. Isaev, V. G. Kostishin, R. I. Shakirzyanov, A. R. Kayumova, V. K. Olitsky and D. V. Salogub, *Tech. Phys.*, 2024, **68**, S552–S561.
9 J. L. Song, Y. Gao, G. G. Tan, Q. k. Man and Z. Wang, *Ceram. Int.*, 2022, **48**, 22896–22905.
10 J. H. Ha, S. Lee, B. Park, J. Lee and I. H. Song, *J. Aust. Ceram. Soc.*, 2020, **56**, 1–11.

11 D. D. Min, J. L. Jiang, Y. C. Qing, X. Y. Gao, G. Hu and M. Zhou, *J. Alloys Compd.*, 2023, **948**, 169817.
12 E. Y. He, T. M. Yan, X. C. Ye, Q. Gao, C. Yang, P. Yang, Y. S. Ye and H. H. Wu, *J. Mater. Sci.*, 2023, **58**, 11647–11665.
13 S. V. R. Rama, *J. Mater. Sci.*, 2022, **33**, 13198–13206.
14 R. A. Sadrolhosseini and M. Naseri, *Prot. Met. Phys. Chem. Surf.*, 2019, **55**, 72–79.
15 A. D. Bamburov, A. A. Markov, I. A. Leonidov and M. V. Patrakeev, *J. Solid State Electrochem.*, 2018, **22**, 899–907.
16 L. J. Xu, Z. Li, F. N. Xiao, Y. C. Zhao, Y. C. Zhou and S. Z. Wei, *Tungsten*, 2022, **5**, 481–502.
17 Y. A. Khalafallah, A. M. Siddig, A. O. Algethami, A. A. Elbadawi and S. A. Mohammed, *Mater. Res. Express*, 2024, **11**, 055003.
18 W. Li, Z. L. Zhang, Y. Y. Lv, Z. Wu, L. Yang, W. X. Zou and Y. H. Zou, *Appl. Surf. Sci.*, 2022, **571**, 151349.
19 X. G. Su, J. Wang, M. J. Han and Y. Q. Liu, *New Chem. Mater.*, 2023, **51**, 157–161, DOI: **10.19817/j.cnki.issn1006-3536.2023.11.051**.
20 H. W. Chen, X. Y. Weng, Z. J. Ma and Z. H. Guan, *Chin. J. Rare Met.*, 2020, **44**, 1339–1344.
21 L. Guo, J. H. Yu, Z. J. Li, P. Wang, Z. J. Ding and B. Du, *J. Magn. Magn. Mater.*, 2013, **44**, 19–22+27.
22 B. Laxmikant and A. Sadhana, *Curr. Appl. Phys.*, 2023, **56**, 47–65.
23 J. Gao, Z. J. Ma, F. L. Liu and X. Y. Weng, *Rare Met.*, 2023, **1**, 254–262.
24 C. Tang, J. Y. Yang, W. B. Deng, Y. H. Bai, B. W. Han, Z. L. Xu, Z. W. Liu, K. Zhao and Y. F. Tang, *Carbon*, 2024, 218118697.
25 Z. J. Ma, C. Y. Mang, J. C. Wang, X. Y. Weng, L. W. Si and Z. H. Guan, *Chin. J. Mater. Res.*, 2017, **12**, 909–917.
26 B. Trinadh, J. Suresh, G. R. Patta, B. K. Vijaya, C. Komali, B. B. Vikram, D. K. Anjani, M. B. Sathish and K. Samatha, *Solid State Commun.*, 2023, **376**, 115360.
27 W. Q. Guo, B. Hong, J. C. Xu, Y. B. Han, X. L. Peng, H. L. Ge, J. Li, H. W. Chen and X. Q. Wang, *Diamond Relat. Mater.*, 2024, 141110699.
28 F. Tian, Y. Gao, A. P. Wang, L. Xiang, Q. K. Man, H. Xu and B. G. Shen, *J. Magn. Magn. Mater.*, 2023, **587**, 171229.
29 C. Wang, N. K. Chen, Y. Y. Xiao, J. H. He, R. Han and N. N. Song, *Ceram. Int.*, 2023, **49**, 36233–36243.
30 S. P. Chi, S. J. Zhu, Y. Zhu, S. J. Feng, X. S. Liu, Q. R. Lv, X. C. Kan and W. Sun, *J. Supercond. Novel Magn.*, 2023, **36**, 1703–1708.
31 Y. X. Xie, Y. Y. Guo, T. T. Cheng, L. B. Zhao, T. Wang, A. Meng, M. Zhang and Z. J. Li, *Chem. Eng. J.*, 2023, **457**, 141205.
32 D. R. Li, X. H. Liang, B. Quan, Y. Cheng, G. B. Ji and Y. W. Du, *Mater. Res. Express*, 2017, **4**, 035604.
33 H. Z. Du, W. M. Zhang, L. Wang, S. Q. Shen, W. W. Dong, Y. F. Hu, S. U. Rehman, H. P. Zou and T. X. Liang, *J. Alloys Compd.*, 2023, **968**, 172129.
34 Y. H. Zhou, G. X. Zhu, P. An and S. Y. Du, *Nanotechnology*, 2020, **31**, 395203.
35 Y. Q. Ge, C. P. Li, G. I. N. Waterhouse, Z. M. Zhang and L. M. Yu, *Ceram. Int.*, 2021, **47**, 1728–1739.